Journal of The Electrochemical Society, **155** (7) B666-B674 (2008)
0013-4651/2008/155(7)/B666/9/$23.00 © The Electrochemical Society

Numerical Study of Heterogeneous Reactions in an SOFC Anode with Oxygen Addition

Yong Hao*,z and David G. Goodwin

Division of Engineering and Applied Science, California Institute of Technology, Pasadena, California 91125, USA

Previous experimental studies have shown that addition of small amounts of oxygen to a hydrocarbon fuel stream can control coking in the anode, while relatively large amounts of oxygen are present in the fuel stream in single-chamber solid oxide fuel cells (SOFCs). In order to rationally design an anode for such use, it is important to understand the coupled catalytic oxidation/reforming chemistry and diffusion within the anode under SOFC operating conditions. In this study, the heterogeneous catalytic reactions in the anode of an anode-supported SOFC running on methane fuel with added oxygen are numerically investigated using a model that accounts for catalytic chemistry, porous media transport, and electrochemistry at the anode/electrolyte interface. Using an experimentally validated heterogeneous reaction mechanism for methane partial oxidation and reforming on nickel, we identify three distinct reaction zones at different depths within the anode: a thin outer layer in which oxygen is nearly fully consumed in oxidizing methane and hydrogen, followed by a reforming region, and then a water–gas shift region deep within the anode. Both single-chamber and dual-chamber SOFC anodes are explored.
 [DOI: 10.1149/1.2907763]

Manuscript submitted November 29, 2007; revised manuscript received March 18, 2008. Available electronically May 2, 2008.

Among the components of a solid oxide fuel cell (SOFC), the anode presents perhaps the most significant technical barrier to creating an efficient, economic, and environmentally friendly technology that makes better use of readily available fuels.[1] Ongoing research has been trying to address these issues by seeking anode materials that possess excellent catalytic, electrochemical, and mechanical properties, and the nickel–zirconia cermet anode is currently the dominant SOFC anode due to its structural stability, small thermal expansion mismatch with popular electrolyte materials, and good catalysis for hydrogen oxidation and steam reforming of hydrocarbon fuels.[1] In particular, the anode-supported membrane-electrolyte assembly (MEA) structure is advantageous for hydrocarbon fuels, because it also serves as a reforming or catalytic partial oxidation catalyst in addition to conducting current.[2] However, it is generally impossible to operate nickel-based anodes on higher hydrocarbon-containing fuels, because nickel also catalyzes the formation of carbon filaments (i.e., coking) from hydrocarbons under reducing conditions,[1] and coking can still occur on Ni catalysts even under thermodynamically noncoking conditions.[3] Formation of carbon deposits on Ni particles is responsible for excessively high activation polarization, which leads to the rapid deterioration of cell performance.[4] For example, Zhan et al. reported that the use of iso-octane causes severe coke buildup on the Ni-yttria-stabilized zirconia (Ni–YSZ) anode and leads to degradation of the anode.[3] Various approaches including steam reforming, addition of oxygen to the fuel stream, and incorporation of dopants into the conventional anode material have been tried to mitigate this problem.[1,2]

The oxygen addition approach is the focus of this paper. For the purpose of carbon removal, it has the advantage (compared with steam reforming) of working well for both methane and higher hydrocarbons, and only a small amount is needed, without substantially affecting the cell efficiency.[1,3] For example, Zhan and Barnett report that a 2% addition to the iso-octane fuel yielded fully stable performance without measurable carbon deposits.[3] While effective for suppressing coke formation for SOFCs in general, mixing oxygen with hydrocarbon fuels (and the ensuing catalytic reactions) in particular is also the working principle of single-chamber SOFCs (SCFCs). More than just the reactant for cathode electrochemistry, oxygen can react with the fuel on the anode side as well, generating hydrogen for anode electrochemistry. Ni-based catalysts have been demonstrated to also exhibit a good activity and selectivity for synthesis gas formation from CH_4/O_2 mixtures.[5] Also, oxidation of the fuel is exothermic, which can help mitigate the cooling effect of the endothermic reforming reaction in the anode bulk, and in some cases can help maintain the operating temperature.[3] Especially in the presence of a large amount of oxygen (as in the case of SCFCs), the heat release becomes so intense that a substantial temperature rise is usually observed experimentally, which in some cases can allow the fuel cell to work steadily without additional external heating (e.g., use of a furnace).[6]

Despite the possible benefits of oxygen addition, current understanding of the detailed reaction mechanism of oxygen with the fuel species in a typical SOFC anode is rather limited due to the complexity of the reactions and the lack of experimental diagnostic methods that could resolve the reactions in the microstructure in situ.

In this paper, the heterogeneous elementary reactions in the anode of an anode-supported MEA with both large (for SCFCs) and small (for dual-chamber SOFCs) oxygen addition are studied using the numerical model we have described previously[7] for a methane-fueled SOFC. The anode-supported structure is chosen to keep with our previous work,[7] in addition to its advantages mentioned above. Although the oxidation of the fuel in general could occur both in the gas phase (i.e., homogeneous) and between the gas phase and the catalyst surface (i.e., heterogeneous),[2] for methane the homogeneous reaction does not play a substantial role for SOFCs until 900°C,[8] which is higher than the normal operating temperature of most SOFCs. Therefore, in this paper we consider heterogeneous chemistry only.

In the existing literature concerning using oxygen for coke prevention in SOFC operation, the role of oxygen in the heterogeneous reactions is not clear,[3] and in the majority of the SCFC studies, its role is vaguely explained as partially oxidizing the hydrocarbon fuel to produce syngas, without any discussion of the reaction pathway.[9] It is a common practice to use mass spectrometry[3,10] or gas chromatography[11] to analyze the outlet gas in an SOFC experiment, which is necessary but far from being sufficient to determine what reactions are actually taking place in the anode.

Studies using fixed-bed reactors provide some useful insights. DeGroote and Froment show the existence of total combustion followed by steam-reforming reactions and water–gas shift reaction in a numerical study of catalytic partial oxidation of methane to syngas over nickel.[12] Ishikara and Takita[5] and Deutschmann and Schmidt[13] carried out a series of experimental and modeling studies concerning surface and gas-phase chemistry on different catalyst metals in a short-contact-time reactor. From these measurements, they developed a multistep, elementary reaction mechanism to describe steam-assisted catalytic partial oxidation of methane in small-channel monolith reactors using Ni supported on alumina. This paper employs the mechanism developed by Deutschmann et al.[14] to study

* Electrochemical Society Student Member.
z E-mail: haoyong@caltech.edu

the anode catalytic chemistry with various amounts of oxygen addition under typical SOFC operating conditions. The reliability of the mechanism has been validated by the work of Hecht et al. for dual-chamber SOFCs[15] and by our previous work for single-chamber SOFCs[16] for cases with and without oxygen addition in the fuel stream. For the purposes of this study, we assume this reaction mechanism provides an adequate description of the catalytic chemistry within an SOFC anode. We show that the reactions in the anode are much more complex than a simple, distributed partial oxidation, and that understanding these reactions (including combustion, reforming, and shift reactions) will be helpful to optimize the anode design. The numerical model used for this paper was originally developed for single-chamber SOFCs, but with the experimental validation of the simulation results,[16] useful conclusions could be drawn for dual-chamber cases as well. However, this mechanism was not designed to predict coking, and so in this study we only discuss cases for which coking is not a problem.

Numerical Model

The two-dimensional (2-D) model used in this study was originally developed for SCFCs running on hydrocarbon fuels, and is described in more detail in Ref. 7. By fitting a small number of parameters, good agreement was achieved between the model's prediction and other independent experimental results. The model describes gas flow and species transport, heat transfer in the gas phase, multicomponent species transport in porous electrodes, and catalytic partial oxidation and reforming chemistry at the anode, and incorporates a Butler–Volmer formalism for electrode kinetics. It is capable of handling both pure ionic and mixed ionic–electronic conductor electrolytes.

In order to facilitate the following discussions, we recapitulate the parts (modules) of the previously developed model essential for this paper.[16] Detailed descriptions can be found in Ref. 16. The gas channel flow module describes the flow of the gas mixture and species transport in the gas chamber of the SCFC. The continuity equation

$$\frac{\partial \rho}{\partial t} + \nabla \cdot (\rho \mathbf{u}) = 0 \qquad [1]$$

momentum equation

$$\frac{\partial \rho \mathbf{u}}{\partial t} + \nabla \cdot (\rho \mathbf{u}\mathbf{u}) = -\nabla p - \frac{2}{3}\nabla (\mu \nabla \cdot \mathbf{u}) + \nabla \cdot \mu[\nabla \mathbf{u} + (\nabla \mathbf{u})^T] \qquad [2]$$

and species conservation equation

$$\frac{\partial \rho Y_k}{\partial t} + \nabla \cdot (\rho \mathbf{u} Y_k + \rho D_{k,m} \nabla Y_k) = 0 \qquad [3]$$

are solved for the 2-D distribution of velocity, density, and species mass fraction fields in the gas surrounding the MEA of the SCFC at steady state. Similarly, within the porous electrodes, the species conservation equation

$$\nabla \cdot \mathbf{j}_k = A_c W_k \dot{s}_k \qquad [4]$$

is solved for the steady-state mass concentrations $\rho_k (k = 1, \ldots, K)$ of the gaseous species in the pores in conjunction with the surface coverage equation

$$\dot{s}_i = 0 \qquad [5]$$

for the coverage percentages $\theta_i (i = 1, \ldots, K_s)$ of the surface species at steady-state, where the mass flux $\mathbf{j}_k$ is calculated by the Dusty-Gas model[17] and both $\dot{s}_k (k = 1, \ldots, K)$ and $\dot{s}_i (i = 1, \ldots, K_s)$ are supplied by the heterogeneous catalytic reaction mechanism developed by Deutschmann et al.[14] For cells with pure ionic conductor electrolyte like yttria-stabilized zirconia (YSZ), the electrochemistry at the electrode–electrolyte interfaces is described by the Butler–Volmer equation

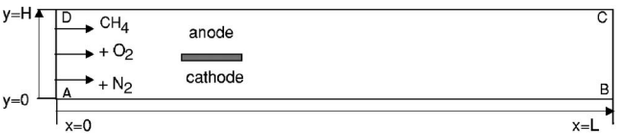

Figure 1. The computational domain for a single-chamber SOFC.

$$i_i = i_0 \left[\exp\left(\frac{\alpha_a \eta_{act} F}{RT} \right) - \exp\left(\frac{\alpha_c \eta_{act} F}{RT} \right) \right] \qquad [6]$$

One of the strengths of this model is that given a heterogeneous reaction mechanism, not only the distribution of gas-phase and surface-phase species within the porous electrodes can be obtained, but the reaction rates of each species and the heat release rates at every point within the electrode can be calculated. Furthermore, surface reactions can be turned on or off depending on the needs of the study. These features are very useful in studying the catalytic kinetics within the anode with oxygen addition in the fuel stream.

However, we have to point out that among the basic assumptions of the model,[7] treating the electrochemistry as a boundary condition for the electrode is a great simplification, for it is well known that the electrochemically active region extends at least 10 μm into the porous electrode.[18] For thin electrodes (e.g., a few tens of micrometers), this is going to be an oversimplification, because electrochemistry over the triple-phase boundary will affect the surface chemistry over a significant portion of the electrode thickness. But for this study, the assumption will not make a major difference in the conclusions, because the anode in an anode-supported MEA is usually around 1 mm thick.

In keeping with our previous work,[16] the anode, electrolyte, and cathode of cells studied in this paper are Ni–YSZ, YSZ, and $Ba_{0.5}Sr_{0.5}Co_{0.8}Fe_{0.2}O_3$, respectively. The temperature is fixed at 750°C (i.e., isothermal), unless stated otherwise. For the single-chamber case, the cell runs in a mixture of methane and oxygen with specified flow rates, with nitrogen being the balance gas. The flow rate of methane is 87 sccm (mL/min at standard conditions), and the ratio of oxygen to nitrogen is always 1:4. The computational domain is shown in Fig. 1 as ABCD with dimensions of $H = 15.9$ mm by $L = 142.9$ mm. Parameters of the computation are listed in Table I.

Results and Discussion

We start with a YSZ cell in the single-chamber configuration at load potential $E = 0.5$ V, where the power density is the highest among all the load potentials. We set the fuel-to-oxygen ratio at the inlet to be the partial oxidation stoichiometry, i.e., CH_4:O_2:N_2 = 2:1:4. The computational grid for the anode is automatically refined by the model, and the finest grid sizes, which occur at the anode–gas and anode–electrolyte interfaces, are around 1 μm, enough for resolving the species profiles. The cell is divided into seven segments of equal lengths along the gas flow direction, and the central one, which is about 6.7 mm from the fuel cell leading edge, is chosen for analyzing the results.

A three-layer structure of the anode reactions.— Figure 2a shows the concentration of gas-phase species within the anode. Although at the inlet of the gas chamber, the molar ratio of oxygen to methane is one-half, over the anode–gas interface (as shown in the figure), this ratio is much lower due to the catalytic reactions in the anode that we discuss shortly. It is also obvious that oxygen penetrates into the anode for only about 25 μm, while methane is abundant throughout the whole anode thickness. The quick depletion of O_2 and the production of H_2O and CO_2 near the anode–gas interface indicate that combustion is taking place, instead of partial oxidation or reforming.

A further study of the reaction rates reveals a three-layer structure of the anode reactions, shown in Fig. 2b. All the rates are normalized by that of methane. That is, the production rate of methane is always −1 (minus sign means "consumed"), and the (relative)

Table I. List of simulation parameters.

Parameters	Value	Unit
Anode		
Thickness	700	μm
Porosity	0.5	—
Tortuosity	3.6	—
Pore radius	0.4	μm
Particle diameter	1.0	μm
Specific catalyst area	7×10^5	m^2/m^3
α_a	1.0	—
α_c	0.4	—
Cathode		
Thickness	10	μm
Porosity	0.3	—
Tortuosity	3.6	—
Pore radius	0.4	μm
Particle diameter	1.0	μm
Specific catalyst area	1.06×10^6	m^2/m^3
α_a	0.6	—
α_c	0.4	—
Electrolyte[a]		
Thickness	15	μm
σ_0	3.6×10^7	Ω^{-1} m^{-1}
E_a	80.0	kJ/mol

[a] The electrolyte ionic conductivity is formulated as $\sigma_i = \sigma_0 T^{-1} \exp(-E_a/R/T)$.

rate for any other species means how many moles of such species is produced for each mole of methane consumed. Our result shows that starting from the anode–gas interface (i.e., the 700 μm line), a combustion zone exists within a 25 μm thick layer where 99% of the O_2 is consumed by combustion with mainly H_2 and CO produced deeper in the anode, rather than CH_4. The syngas consumed in the combustion zone is generated by the methane wet reforming zone extending from 675 to 350 μm and the water–gas shift zone that takes up the rest of the anode thickness. The reactions and demarcation of different zones in the anode are discussed as follows.

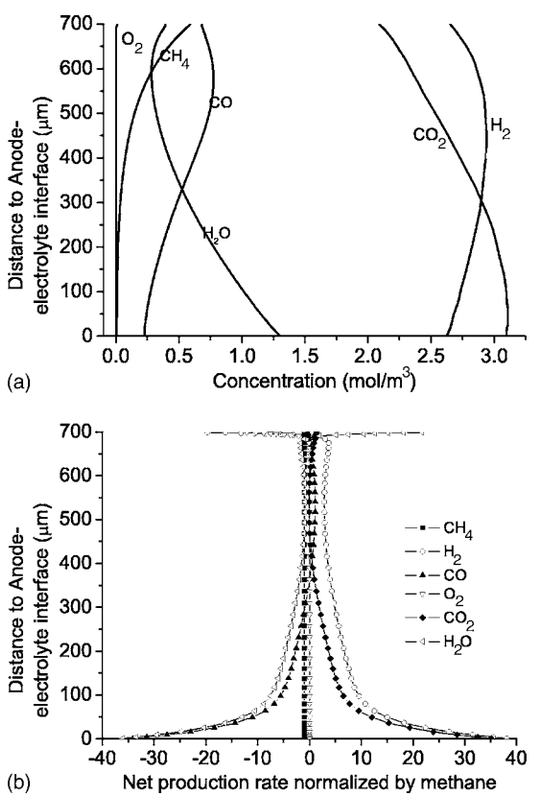

Figure 2. Concentration and net production rates of gas species in the anode at peak-power condition: (a) molar concentration and (b) net production rate relative to methane (dimensionless).

Table II. Possible reactions in an SOFC anode.

Reaction name	Symbol	Reaction equation	ΔQ (kJ/mol)
Methane wet reforming	MWR	$CH_4 + H_2O = 3H_2 + CO$	226.059
Methane dry reforming	MDR	$CH_4 + CO_2 = 2H_2 + 2CO$	258.676
Water–gas shift	WGS	$CO + H_2O = H_2 + CO_2$	−32.618
Combustion of methane	CMM	$CH_4 + 2O_2 = 2H_2O + CO_2$	−802.95
Combustion of hydrogen	CMH	$H_2 + 0.5\ O_2 = H_2O$	−249.098
Combustion of CO	CMC	$CO + 0.5\ O_2 = CO_2$	−281.716

Decomposition of the global reaction.— The calculated reaction rates (as in Fig. 2b) indicate that the chemical reaction within the anode is very complicated and may involve many concurrent processes. For example, our result shows that the global reaction at 1 μm beneath the anode–gas interface involves the simultaneous combustion of methane, hydrogen, and carbon monoxide. Furthermore, the adjacent reaction zones influence each other through both mass- and energy-transport processes. For example, the combustion zone consumes the syngas produced by the other two zones but supplies heat to the reforming reactions because this zone is exothermic. Such complication in kinetics requires deciphering the global reaction through a simpler and quantitative way, and this interpretation could provide more useful insights.

Based on the relative reaction rates discussed above, the global reaction at any point in the anode can be expressed in a general form

$$CH_4 + \alpha H_2 + \beta CO + \gamma O_2 + \varepsilon CO_2 + \delta H_2O = 0 \qquad [7]$$

However, we need to reiterate that the global reaction expressed by the production and consumption of the gas-phase species is just the net result of the multistep heterogeneous elementary reaction mechanism. The actual reactions are assumed to proceed between the gas phase and surface phase, and never in the gas phase alone. The heterogeneous reactions are connected to electrochemistry by way of the gas-phase species, and the heat effect within the anode is more easily calculated by the change of enthalpies of the gas-phase species. Therefore it is convenient to study the reactions in the anode through the formal expression Eq. 7.

Here we try to decompose this global reaction into simpler reactions (listed in Table II) that could possibly occur in the anode under SOFC operating conditions and study the functionality of different reaction zones within the anode for the operation of the SOFC. In Table II all the reactions can be written in a uniform format

$$\sum_{k=1}^{6} \nu_k A_k = 0 \qquad [8]$$

where A_k is the kth gas-phase species in vector (CH_4, H_2, CO, O_2, CO_2, H_2O) and ν_k is the corresponding coefficient. Also, each listed reaction could have a different extent of progress. Therefore, the decomposition of the global reaction amounts to finding a linear combination of the reactions in Table II

$$CH_4 + \alpha H_2 + \beta CO + \gamma O_2 + \varepsilon CO_2 + \delta H_2O = 0$$

$$\Leftrightarrow$$

$$a \cdot \text{MWR} + b \cdot \text{MDR} + c \cdot \text{WGS} + d \cdot \text{CMM} + e \cdot \text{CMH} + f \cdot \text{CMC} \quad [9]$$

by solving the matrix equation

$$A\mathbf{x} = \mathbf{b} \quad [10]$$

where

$$A = \begin{pmatrix} 1 & 1 & 0 & 1 & 0 & 0 \\ -3 & -2 & -1 & 0 & 1 & 0 \\ -1 & -2 & 1 & 0 & 0 & 1 \\ 0 & 0 & 0 & 2 & 0.5 & 0.5 \\ 0 & 1 & -1 & -1 & 0 & -1 \\ 1 & 0 & 1 & -2 & -1 & 0 \end{pmatrix}, \quad \mathbf{x} = \begin{pmatrix} a \\ b \\ c \\ d \\ e \\ f \end{pmatrix},$$

$$\mathbf{b} = \begin{pmatrix} 1 \\ \alpha \\ \beta \\ \gamma \\ \varepsilon \\ \delta \end{pmatrix}$$

for the unknown (positive) coefficients *a*–*f*.

Although methane partial oxidation is frequently reported in SCFC literature, it is not listed in the table because our results do not support its existence anywhere in the anode, even under the partial-oxidation stoichiometry of CH_4:O_2 = 2:1. The reason is discussed shortly. Another note is that because the catalytic reaction mechanism[14] used for this study is not designed to predict coking, we assume that there are no reactions involving solid carbon either. The reaction heat of the six possible reactions in Table II is calculated at the simulation temperature by CANTERA.[19]

In Eq. 10, matrix A only has three nonzero eigenvalues, which means only three equations in Table II are independent and that the solution for *a*–*f* is nonunique. In fact, there are three dependent relations among these reactions

$$\text{MWR} = \text{MDR} + \text{WGS} \quad [11]$$

$$\text{CMC} = \text{WGS} + \text{CMH} \quad [12]$$

$$\text{CMM} = 2\text{WGS} + 4\text{CMH} + \text{MDR} \quad [13]$$

Therefore, the three independent reactions can be picked as methane dry reforming (MDR), water-gas shift (WGS), and combustion of hydrogen (CMH), and the global reaction can be decomposed into a unique linear combination of these reactions, i.e.

$$CH_4 + \alpha H_2 + \beta CO + \gamma O_2 + \varepsilon CO_2 + \delta H_2O = 0$$

$$\Leftrightarrow$$

$$\text{MDR} + c \cdot \text{WGS} + e \cdot \text{CMH} \quad [14]$$

The coefficient for MDR is 1 because it is the only reaction among the three that contains methane. By comparison of coefficients, we obtain

$$e - c - 2 = \alpha \quad [15]$$

$$c - 2 = \beta \quad [16]$$

$$0.5e = \gamma \quad [17]$$

$$1 - c = \epsilon \quad [18]$$

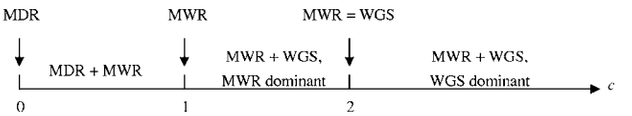

Figure 3. Change of syngas production reactions in the global reaction with respect to the decomposition coefficient *c*.

$$c - e = \delta \quad [19]$$

and the solution is

$$c = \beta + 2, \quad e = 2\gamma \quad [20]$$

Although Eq. 15, 18, and 19 appear to be redundant, they are inherently consistent with Eq. 16 and 17 based on the conservation of C, H, and O.

So the global reaction equation can be written as the superposition of the following three reactions

$$CH_4 + CO_2 = 2H_2 + 2CO \quad [21a]$$

$$CO + H_2O = H_2 + CO_2 \quad [21b]$$

$$H_2 + 0.5O_2 = H_2O \quad [21c]$$

with Reactions 21b and 21c multiplied by the corresponding coefficients *c* and *e*, respectively. Reactions 21a and 21b account for the syngas production, while Reactions 21b and 21c account for the syngas combustion. In the following discussion, we call Eq. 21a-21c the basic decomposition of the global Reaction 7.

There are three special cases for Eq. 21a-21c that facilitate further discussion: (*i*) When O_2 is depleted, $\gamma = 0$ in Eq. 14, and the basic decomposition is only Eq. 21a and 21b. Because oxygen is depleted in the combustion zone, this case applies to the reaction zones deeper into the anode cermet. (*ii*) When H_2O is depleted, $\delta = 0$ in Eq. 14, and it follows that $c = e$ (by Eq. 19). Because water is generated within the combustion zone, the case of water depletion can only occur in other reaction zones, where there is no oxygen. Thus, $\gamma = e/2 = 0$ (by Eq. 20), $\alpha = -2$ (by Eq. 15), $\epsilon = 1$ (by Eq. 18), and $\beta = -2$ (by Eq. 16). Therefore the global reaction is uniquely decomposed as the dry reforming of methane. (*iii*) When $\beta = -1$ (or $c = 1$), Eq. 21a and 21b may be combined into methane wet reforming reactions; when $\beta = 0$ (or $c = 2$), the basic decomposition can be written as one methane wet reforming followed by one water–gas shift reaction, i.e., they are equally important in the global reaction. The change of syngas production reactions with respect to coefficient *c* is illustrated in Fig. 3.

Last, the application of the dependent relations Eq. 11-13 to the basic decomposition Reactions 21a-21c will yield an infinite number of possible decompositions of the global reaction. Because the global Reaction 7 is the net result of a set of multistep heterogeneous reactions,[14] it would be extremely complicated and unnecessary to determine which decompositions are more likely than others. On the contrary, it is sufficient to use the basic decomposition to interpret the reactions in the anode because it accounts for the production and consumption of the syngas.

Reaction zones at different load potentials.— The layered structure of the anode reactions under the peak-power condition can be illustrated by the plot of coefficients *c* and *e* in Fig. 4. It shows that the combustion component of the global reaction only exists from 700 to 660 μm, and the reactions in the rest of the anode thickness are methane wet reforming and water–gas shift reactions. In the combustion zone, due to the relative abundance of H_2O, the last two reactions are also possible. However, notice that *c* is smaller than *e* in the region from 700 to 675 μm. By the dependent relations 11-13, it is more appropriate to explain the global reaction in this region as the combustion of H_2, CO, and CH_4, with the combustion of H_2 being the dominant reaction. The region between 675 and 660 μm is a transitional zone with the global reaction shifting from combustion

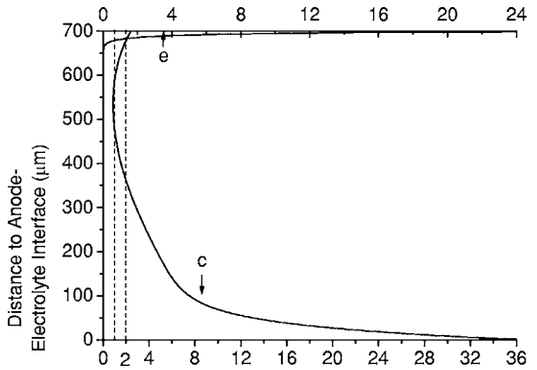

Figure 4. Coefficients *c* and *e* in the basic decomposition under the peak-power condition.

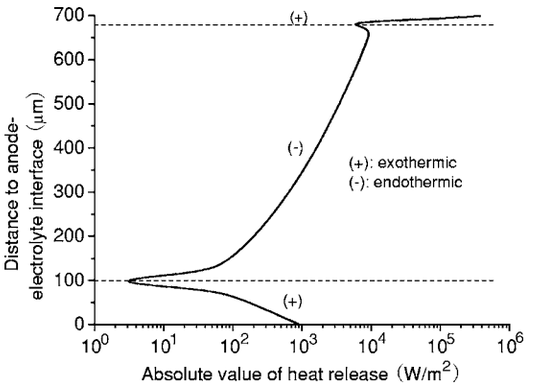

Figure 6. Heat release profile along the anode depth under the peak-power condition.

to methane wet reforming and water–gas shift reactions. Based on the criteria in Fig. 3, the region between 660 and 350 μm is dominated by methane wet reforming, and the region below 350 μm is dominated by the water–gas shift reaction.

In connection with the reaction zones, the calculated coverage fraction of the surface species shows that 20–25% of the Ni surface is covered. Among them, the species that have significant coverages are plotted in Fig. 5. Generally speaking, the coverage of the O(s) (where "s" means surface) species follows the concentration of H_2O, indicating that the steam generated by electrochemistry has a significant influence on the surface reactions. Also, the coverage of carbon over the Ni surface is consistently close to zero throughout the anode thickness, thus ensuring that the calculation stays outside the coking region.

The basic decomposition also makes the understanding of the heat effect of the global reaction very straightforward. Among the three independent reactions we picked for the decomposition, methane dry reforming is strongly endothermic, while water–gas shift and hydrogen combustion are weakly and strongly exothermic, respectively. By taking the absolute reaction rate of methane into account, the heat release rate along the thickness of the anode can be calculated and plotted in Fig. 6, in which endothermic and exothermic regions are marked by (−) and (+), respectively, and a log-scale is used due to the huge difference in the magnitude of heat release in different zones. The figure shows that the combustion zone gives off much heat, while the heat absorption in the reforming zone deeper into the anode is less intense due to the decrease in total reaction rate. The combustion heat is beneficial to the reforming reaction. The heat release profile reinforces the argument of the three-layer structure, i.e., a highly exothermic combustion zone close to the anode–gas interface, a methane wet reforming zone in the middle, and water–gas shift zone next to the anode–electrolyte interface. Close to the anode–electrolyte interface, the transition from endothermic to exothermic occurs at 100 μm instead of 350 μm (i.e., the boundary between wet reforming and water–gas shift zones) because the reaction heat of the shift reaction is much weaker than that of the reforming reaction.

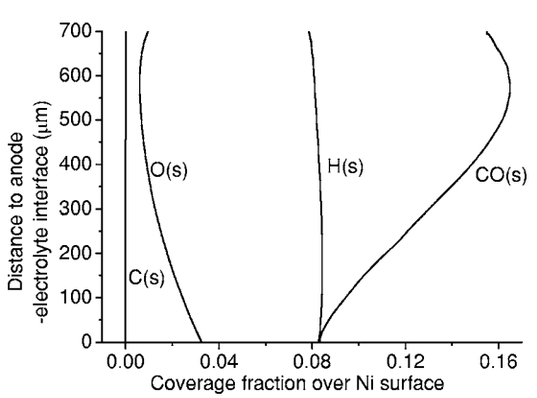

Figure 5. Coverage fractions of selected surface species under the peak-power condition.

The three-layer structure of the anode is in agreement with the indirect route of the syngas production suggested by Ishihara and Takita[5] in the study of methane partial oxidation with oxygen-permeating ceramic membrane reactors, for which combustion of CH_4 to CO_2 and H_2O is followed by the reforming reaction of CH_4 with H_2O and CO_2–CO and water–gas shift conversions. The 25 μm thick combustion layer mimics the reactor entrance, where an extremely rapid variation of temperature, velocity, and transport coefficients occurs.[5] The heat release in this layer not only provides the heat for the endothermic steam reformation,[2] but also leads to a significant temperature rise, verified both experimentally by several groups[6,20-22] and numerically by our previous work.[16]

We also need to reiterate that the interpretation of syngas production by way of methane partial oxidation is inappropriate anywhere within the anode, as shown by the discussions about the three-layer structure. Oxygen is quickly depleted within the combustion layer, which makes partial oxidation of methane impossible in the other two layers. Meanwhile, in the combustion layer itself, the reaction of oxygen is primarily with hydrogen rather than methane, also ruling out the possibility of partial oxidation. Even if the superposition of all reaction rates at each point within the anode cermet would result in some formulation close to a "global" partial oxidation reaction, the formalism would be very blurry and does not help to explain the mechanism for the detailed reactions within the anode cermet.

Next, we switch from the peak-power condition to short-circuit condition (where the load potential $E = 0.0$ V) to study the difference in reaction zones. The reasons for this are that one major difference between the reactor and an SOFC anode is the contribution of steam by electrochemistry which proceeds at the maximum rate under such a condition, and that H_2O plays an important role in both reforming and water–gas shift reactions. Therefore, the layered structure of the anode in the presence of significant electrochemical reactions needs further study under a different condition from what has been previously discussed.

The gas concentrations in the anode under the short-circuit condition are plotted in Fig. 7. By comparison, a larger amount of H_2O is produced by electrochemistry, providing more steam for the reforming of methane and the water–gas shift reactions. As a result, the concentration of methane decays more rapidly with depth into the anode, and the concentration of CO_2 is higher while that of CO is considerably lower compared with the peak-power case. The con-

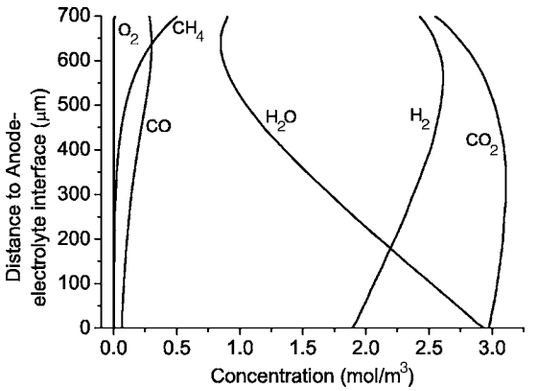

Figure 7. Molar concentration of gas-phase species in the anode under the short-circuit condition.

centration of H_2 is lower due to the increased consumption by electrochemistry, verified by the significantly elevated concentration of H_2O. The existence of abundant water vapor also accounts for the lower concentrations of CO and CH_4. The coefficients *c* and *e* for the basic decomposition are plotted in Fig. 8. It shows that the combustion part is very similar to that under peak-power conditions, while with the higher H_2O concentration, the water–gas shift reaction takes up an even greater portion of the anode thickness.

In Fig. 7, there is a minimum for H_2O at about 640 μm and a maximum for H_2 at about 560 μm. A calculation of mass fluxes of species shows that the steam produced by the combustion layer never goes downward beyond the 640 μm line, and the H_2 and CO generated by this part of the steam diffuse back to the combustion zone to be fully oxidized. The steam generated by electrochemistry goes upward until the 640 μm line. The H_2 it generates through reforming and shift reactions partly diffuses to the combustion layer and partly diffuses back to the anode–electrolyte interface, where it is converted to H_2O by electrochemistry again. This means that the H_2 for electrochemistry is not directly relevant to the combustion zone but is solely produced by internal reforming. The major role of O_2 is supplying the heat to steam reforming by way of full oxidation of the syngas. The combustion makes the gas mixture in the flow channel on the anode side increasingly fuel-rich so that more oxygen is needed by the downstream part of the fuel cell, shifting the optimum fuel-to-oxygen ratio toward the fuel-lean condition.[7] For this reason, the working principle of SCFC can be explained by neither the partial oxidation of methane, nor some nominal "global" reaction for the whole anode obtained by superposing the reactions at different depths in the anode, because different regions of the anode are responsible for different functionalities.

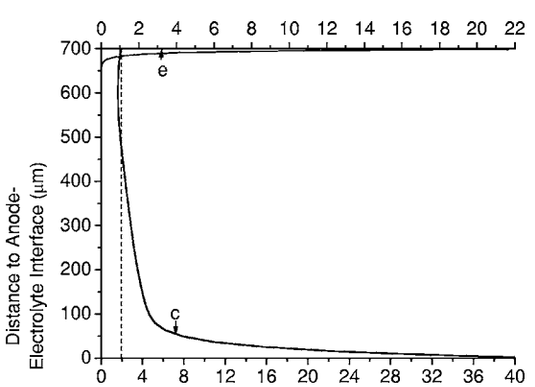

Figure 8. Coefficients *c* and *e* in the basic decomposition under short-circuit condition.

The concentrations of CH_4, H_2, O_2, and H_2O are plotted vs depth into the anode in Fig. 9 at both load potentials (0.5 and 0.0 V). It is obvious that the change in load potential has little influence on the O_2 consumption and thus the combustion zone, while the consumption of CH_4 and the production of H_2 are greatly influenced by the concentration of H_2O, which is in turn determined mainly by load potential.

We also find that at both load potentials, the total heat release at each point along the fuel cell, which is obtained by superposing the reaction heat point-wise along the anode thickness, strongly depends on the consumption rate of the oxygen. The total heat release along the fuel cell under short-circuit conditions is plotted in Fig. 10. The heat release is the highest at the fuel cell leading edge, because O_2 concentration is the highest. It drops sharply toward the trailing edge due to both the depletion of O_2 and the endothermic reactions deeper in the anode.

Besides the heat effects of the reactions within the anode, the charge-transfer process at the anode–electrolyte interface also makes a considerable contribution to the total heat release. Figure 11 plots the comparison between the heating power of the catalytic reactions within the anode and that of the charge-transfer process at the anode–electrolyte interface, defined as the product of the local power density and charge-transfer overpotential, both computed by the model. The comparison shows that except at the fuel cell leading edge, the charge-transfer heating power is comparable to that of the catalytic reactions. Therefore, the heat generation of both the combustion zone and the charge-transfer process are important heat sources for sustaining the endothermic reactions within the anode cermet.

Last, we also simulated the SOFC under open-circuit condition, and our result indicates that while the combustion zone is similar to the two cases discussed above, serious coking shows up within the anode. Because the reaction mechanism used in this work is not validated against carbon formation, we do not quantitatively discuss the open-circuit case. However, based on the discussion above, we can understand that under open-circuit condition, there is no water vapor produced by electrochemistry, and oxygen cannot penetrate very deep into the anode, so that coking is very probable within the anode. Oxygen is useful to prevent coking in the combustion zone.

The reaction zones under general operating conditions.— Our study also shows that the layered structure of the anode reactions exists for a wide range of operation parameters, including voltage (0 V to open circuit), temperature (550–800°C at least), and the fuel-to-oxygen ratio (0.5–2.0 at least), and the similarity is that the combustion zone always exists within a thin layer beneath the anode–gas interface, and there is always a layered structure of reaction zones. However, there are quantitative differences depending on specific conditions. For example, at lower voltages (e.g., short circuit), methane is depleted faster due to the higher concentration of H_2O produced by electrochemistry, and therefore the reforming zone is narrower, while the water–gas shift zone is wider; at smaller fuel-to-oxygen ratios (e.g., stoichiometry for methane combustion), the combustion zone can be much wider due to the abundant oxygen, resulting in a very low H_2 concentration and power output. As for temperature, although the mechanism we use here does not apply above 800°C, it can be inferred that the combustion zone will become wider with temperature because the selectivity of the nickel anode goes down, which will result in a loss of power output. One example in case is Hibino's earlier study of SCFCs,[23-25] in which the furnace temperature is 950°C and the fuel cell temperature should be well above 1000°C. The low power output should be partly accounted for by the combustion zone under such high temperatures.

Dual-chamber SOFC anode with a small O_2 addition.— Besides the single-chamber case, we also investigated the dual-chamber SOFC in a button cell configuration (Fig. 12) with 5% addition of oxygen in the methane fuel stream in the anode chamber at 800°C. Although the anode catalytic reaction mechanism is not designed to predict coking, this study certainly brings more insight into the role

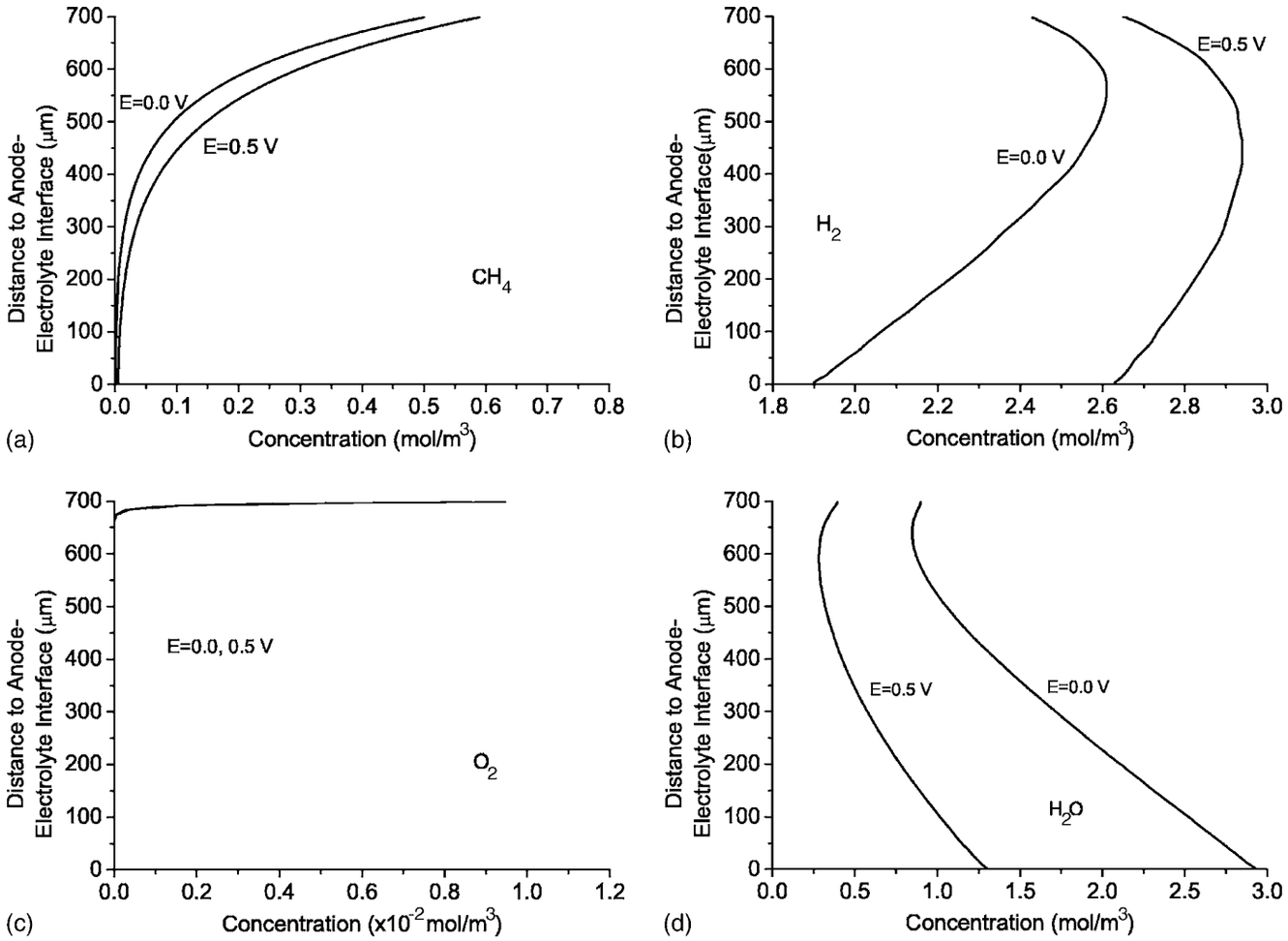

Figure 9. Concentration of selected species within the anode at different load potentials: (a) CH_4, (b) H_2, (c) O_2, and (d) H_2O.

that oxygen plays in preventing coking. The cathode chamber was supplied with air at a flow rate of 250 sccm. The load potential was 0.5 V, and all other parameters were the same as the single-chamber case.

Figure 13 shows the species profile and net production rates along the centerline in the button cell. In this case, the reaction zones in the anode are more complicated than the single-chamber case. One major difference is that there is no combustion layer. Starting from the anode–gas interface, there is a very thin layer of about 5 μm in which methane is partially oxidized by ambient O_2 to syngas and water, and the heat release is positive. This process quickly depletes most of the oxygen entering the anode, and the water and CO_2 produced by this oxidation enables reforming of the methane to occur in the next 15 μm or so. The water production rate changes from positive to negative and the CO_2 rate is also negative

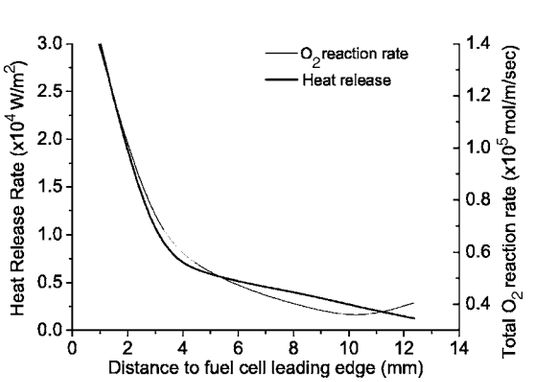

Figure 10. Total heat release and O_2 reaction rate of the fuel cell along the flow direction under short-circuit condition.

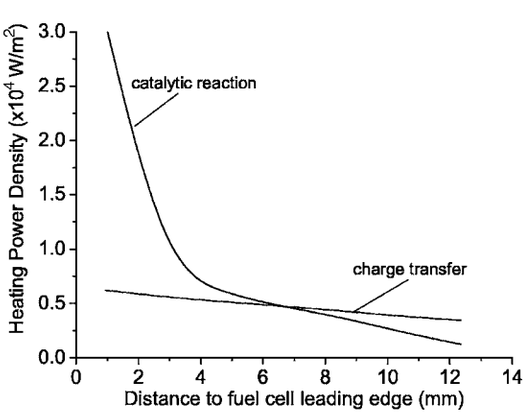

Figure 11. Comparison of the heating effect of the catalytic reactions within the anode and that of the charge-transfer process at the anode–electrolyte interface.

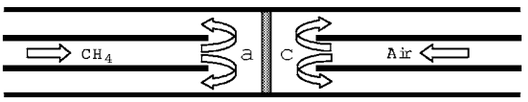

Figure 12. The dual-chamber SOFC simulated in a button cell configuration: (a) anode and (c) cathode.

while H_2 and CO are being produced. In this region, the heat release is negative. From 650 to 450 μm, no significant reaction happens because H_2O generated by the partial oxidation is consumed. From 450 to 400 μm, CH_4 and CO_2 start to be consumed again and syngas is produced, but the concentration of H_2O is still close to zero in this region. Therefore the reaction is "dry" reforming. The layer between 400 and 100 μm is a regular reforming region in which H_2O produced by electrochemistry converts CH_4 to syngas. Finally, in the last 100 μm before the electrolyte, methane is almost depleted and the dominant chemistry is a water–gas shift, with the steam coming from the electrolyte and the CO coming from the dry-reforming and regular reforming layers above.

Compared with the case with no oxygen addition, the presence of oxygen generates heat and steam within the 20 μm layer beneath the anode–gas interface. The increase of cell temperature due to the heat release and the steam reforming of methane are both beneficial to prevent coking. Also, the power output is not influenced because the amount of oxygen is too small. We find that 10% oxygen (by volume) is needed to reduce the power output by 1%, thus validating the conclusions of Zhan and Barnett.[3] The discharge characteristics plot is shown in Fig. 14.

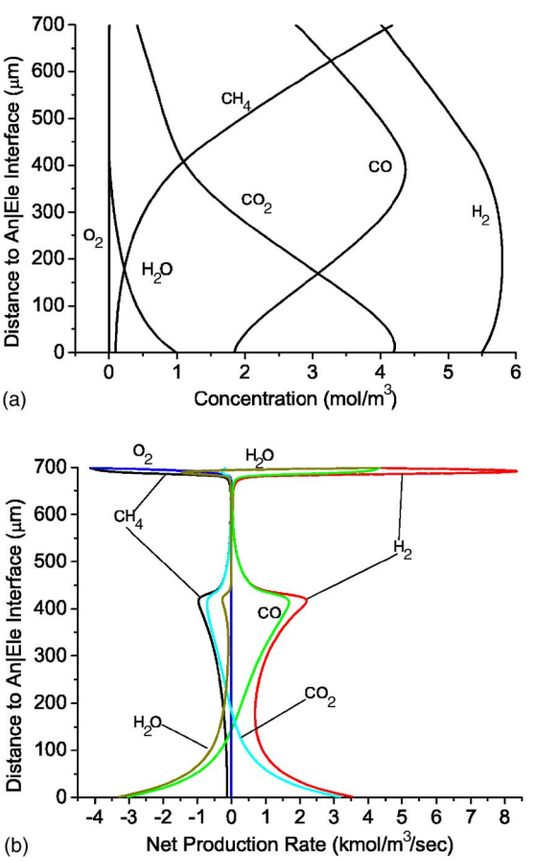

Figure 13. (Color online) Concentrations and net production rates of gas-phase species in a dual-chamber SOFC anode: (a) molar concentration and (b) net production rate.

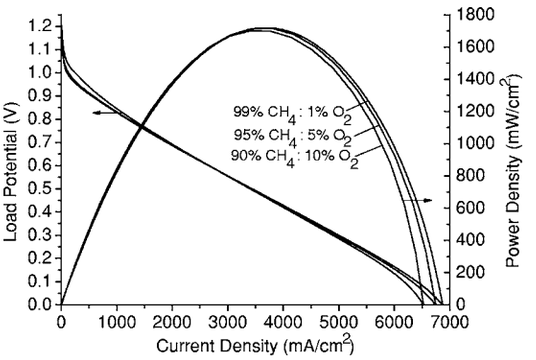

Figure 14. Simulated discharge characteristics of a dual-chamber fuel cell running on methane with small oxygen addition in the anode chamber.

Conclusions

Through simulation of an SOFC anode with large oxygen addition, we find that three distinct regions exist in general, which starting from the anode–gas interface, are a thin outer layer in which oxygen is nearly fully consumed in oxidizing methane and hydrogen, followed by a wet reforming region, and then a region with water–gas shift adjacent to the anode–electrolyte interface. A scheme is developed to decompose the global reaction into simpler reactions for an easy interpretation of the characteristics of different reaction zones and an easy calculation of the heat effect.

Our results show that the consumption rate of O_2 is virtually not influenced by the load potential of the fuel cell, and the role of O_2 is to generate heat and water steam in the combustion zone, both of which are necessary for operating the SOFC and the prevention of coking. Due to the existence of the combustion zone, the heat release at most locations along the fuel cell length direction is positive, making it a major contributor of the heat needed to sustain the fuel cell temperature and the endothermic reactions for generating the syngas.

Our results also indicate that partial oxidation of methane is unlikely to be the major factor for either syngas production or cell heating. Rather, the hydrogen for electrochemistry is mostly produced by internal reforming, even in the presence of abundant oxygen (i.e., the single-chamber cases), and cannot be explained by a simple, global partial oxidation reaction. The heat effect is mainly due to the full rather than partial oxidation of both syngas and methane even under fuel-rich conditions.

For situations with a small O_2 addition, as is the case of a dual-chamber SOFC anode, the combustion zone actually vanishes and O_2 is more quickly depleted by partial oxidation of methane and syngas within a narrower region compared with the single-chamber case. However, the role of O_2 for generating heat and steam is similar. Our result verifies that the existence of a small amount of O_2 (up to 10 vol %) has little impact on the power density, and thus a small O_2 addition in the fuel stream could effectively prevent coking while not significantly affecting the electrical performance.

Acknowledgments

This work was partly supported by the Defense Advanced Research Projects Agency (DARPA) under grant no. N66001-01-1-8966 and partly by the Office of Naval Research under grant no. N00014-05-1-0339. We greatly appreciate the constructive suggestions from S. M. Haile, Z. Shao, C. Pantano, W. Lai, and J. Mederos.

California Institute of Technology assisted in meeting the publication costs of this article.

References

1. A. Atkinson, S. Barnett, R. J. Gorte, J. T. S. Irvine, A. J. McEvoy, M. Mogensen, S. C. Singhal, and J. Vohs, *Nat. Mater.*, **3**, 17 (2004).
2. R. J. Kee, H. Y. Zhu, and D. G. Goodwin, *Proc. Combust. Inst.*, **30**, 2379 (2005).

3. Z. L. Zhan and S. A. Barnett, *Science*, **308**, 844 (2005).
4. W. Z. Zhu and S. C. Deevi, *Mater. Sci. Eng., A*, **362**, 228 (2003).
5. T. Ishihara and Y. Takita, *Catal. Surv. Jpn.*, **4**, 125 (2000).
6. Z. P. Shao, S. M. Haile, J. Ahn, P. D. Ronney, Z. L. Zhan, and S. A. Barnett, *Nature (London)*, **435**, 795 (2005).
7. Y. Hao and D. G. Goodwin, *J. Electrochem. Soc.*, **154**, B207 (2007).
8. K. M. Walters, A. M. Dean, H. Y. Zhu, and R. J. Kee, *J. Power Sources*, **123**, 182 (2003).
9. X. Jacques-Bedard, T. W. Napporn, R. Roberge, and M. Meunier, *J. Power Sources*, **153**, 108 (2006).
10. E. P. Murray, S. J. Harris, J. Liu, and S. A. Barnett, *Electrochem. Solid-State Lett.*, **9**, A292 (2006).
11. T. Hibino, A. Hashimoto, M. Yano, M. Suzuki, S. Yoshida, and M. Sano, *J. Electrochem. Soc.*, **149**, A133 (2002).
12. A. M. DeGroote and G. F. Froment, *Appl. Catal., A*, **138**, 245 (1996).
13. O. Deutschmann and L. D. Schmidt, *AIChE J.*, **44**, 2465 (1998).
14. H. Y. Zhu, R. J. Kee, V. M. Janardhanan, O. Deutschmann, and D. G. Goodwin, *J. Electrochem. Soc.*, **152**, A2427 (2005).
15. E. S. Hecht, G. K. Gupta, H. Y. Zhu, A. M. Dean, R. J. Kee, L. Maier, and O. Deutschmann, *Appl. Catal., A*, **295**, 40 (2005).
16. Y. Hao, Z. P. Shao, J. Mederos, W. Lai, D. G. Goodwin, and S. M. Haile, *Solid State Ionics*, **177**, 2013 (2006).
17. E. A. Mason and A. P. Malinauskas, in *Gas Transport in Porous Media: The Dusty-Gas Model*, American Elsevier, New York (1983).
18. W. Kim, A. V. Virkar, K. Z. Fung, K. Mehta, and S. C. Singhal, *J. Electrochem. Soc.*, **146**, 69 (1999).
19. D. G. Goodwin, in *Chemical Vapor Deposition XVI and EUROCVD 14*, M. Allendorf, F. Maury, and F. Teyssandier, Editors, PV 2003-08, p. 155, The Electrochemical Society Proceedings Series, Pennington, NJ (2003).
20. T. Hibino, A. Hashimoto, T. Inoue, J. Tokuno, S. Yoshida, and M. Sano, *J. Electrochem. Soc.*, **148**, A544 (2001).
21. T. Suzuki, P. Jasinski, V. Petrovsky, H. U. Anderson, and F. Dogan, *J. Electrochem. Soc.*, **151**, A1473 (2004).
22. T. W. Napporn, X. Jacques-Bedard, F. Morin, and M. Meunier, *J. Electrochem. Soc.*, **151**, A2088 (2004).
23. T. Hibino, S. Q. Wang, S. Kakimoto, and M. Sano, *Solid State Ionics*, **127**, 89 (2000).
24. T. Hibino, H. Tsunekawa, S. Tanimoto, and M. Sano, *J. Electrochem. Soc.*, **147**, 1338 (2000).
25. T. Hibino, A. Hashimoto, T. Inoue, J. Tokuno, S. Yoshida, and M. Sano, *J. Electrochem. Soc.*, **147**, 2888 (2000).